

Physical properties of CeIrSi with trillium-lattice frustrated magnetism

F. Kneidinger,¹ I. Zeiringer,² A. Siderenko,¹ E. Bauer,¹ H. Michor,¹ P. Rogl,² and J. G. Sereni³

¹*Institute of Solid State Physics, TU Wien, A-1040 Wien, Austria*

²*Institut für Materialchemie, Universität Wien, A-1020 Wien, Austria*

³*Low Temperature Division CAB-CNEA, CONICET, 8400 S.C. de Bariloche, Argentina*



(Received 16 July 2019; revised manuscript received 6 October 2019; published 31 October 2019)

Magnetic (χ), transport (ρ), and heat capacity (C_m) properties of CeIrSi are investigated to elucidate the effect of geometric frustration in this compound with trillium type structure because, notwithstanding its robust effective moment, $\mu_{\text{eff}} \approx 2.46 \mu_B$, this Ce-lattice compound does not undergo a magnetic transition. In spite of that it shows broad $C_m(T)/T$ and $\chi(T)$ maxima centered at $T_{\text{max}} \approx 1.5$ K, while a $\rho \propto T^2$ thermal dependence, characteristic of electronic spin coherent fluctuations, is observed below $T_{\text{coh}} \approx 2.5$ K. Magnetic field does not affect significantly the position of the mentioned maxima up to ≈ 1 T, though $\chi(T)$ shows an incipient structure that completely vanishes at $\mu_0 H \approx 1$ T. Concerning the $\rho \propto T^2$ dependence, it is practically not affected by magnetic field up to $\mu_0 H = 9$ T, with the residual resistivity $\rho_0(H)$ slightly decreasing and $T_{\text{coh}}(H)$ increasing. These results are compared with the physical properties observed in other frustrated intermetallic compounds.

DOI: [10.1103/PhysRevB.100.134442](https://doi.org/10.1103/PhysRevB.100.134442)

I. INTRODUCTION

The lack of magnetic order in lattice arrangements of robust magnetic moments leads to ground states with high density of low energy excitations. Two typical scenarios allow us to prevent the development of magnetic order: (i) the weakness of the magnetic interactions or (ii) the frustration of antiferromagnetic interactions. In the former, cerium magnesium nitrate hydrate (CMN) is the exemplary case because it remains paramagnetic down to ≈ 2 mK due to the large Ce-Ce spacing ($d_{\text{Ce-Ce}} \approx 11 \text{ \AA}$ [1]) and the absence of conduction electrons. In the latter context, two circumstances may produce frustration; one due to geometrical constraints like triangular (2D) or tetrahedral (3D) spin lattices, or because of the competition between nearest (nn) and next nearest neighbors (nnn) interactions [2]. The pyrochlore structure of the $\text{Dy}_2\text{Ti}_2\text{O}_7$ spin-ice [3] is an exemplary system for the 3D-tetrahedral coordination case, whereas some 2-2-1 (see, e.g., $\text{Ce}_{2.15}(\text{Pd}_{0.5}\text{Ag}_{0.5})_{1.95}\text{In}_{0.9}$ discussed in Ref. [4]) compounds showing a network of triangles and squares exhibit magnetic frustration in their basal (2D) planes. Finally, the competition between nn and nnn interactions can be exemplified by Yb_4LiGe_4 [5].

Among the crystalline structures favoring 3D geometric frustration, the cubic trillium (LaIrSi-type) structure [6–8] should provide an ideal playground for a study of the competition between RKKY interactions and frustration effects. Several light rare earth-iridium-silicides (REIrSi, RE = rare earth) are members of this structure type as well as EuPtSi which recently attracted significant attention [9–13].

Ternary intermetallics REIrSi have been intensely studied in the past few decades. The respective crystal structure depends on the distinct rare earth element. Compounds with RE = La, Ce, Pr, and Nd exhibit the cubic chiral LaIrSi structure type (space group $P2_13$) [6,7], where inversion symmetry is missing. This structure type is a ternary ordered version of the binary SrSi_2 type (space group $P4_132$). Due to ordering

of the Ir and Si atoms in LaIrSi, symmetry is lowered, as evidenced from the respective space groups. The iridium and silicon atoms build up a three-dimensional [IrSi] network with rather short Ir-Si distances, inferring strong covalent bonding [8]. On the other hand, distances between rare earth ions and Si or Ge are much larger, evidencing a much weaker bonding [8]. Silicides with heavy rare earth elements (RE from Gd to Lu), however, are crystallizing in the orthorhombic TiNiSi structure (space group $Pnma$) [14].

While CeIrSi was characterized from temperature dependent susceptibility data as a paramagnet without magnetic ordering down to 1.5 K [8], for NdIrSi, Chevalier *et al.* [7] reported a ferromagnetic ground state below $T_C = 10$ K from a spontaneous magnetization.

In the present study we aim a thorough characterization of CeIrSi by means of its thermodynamic and transport properties investigation in order to elucidate the effect of geometric frustration with respect to ground state properties of this compound. Because of distinct features of the trillium structure, a weaker Ce-Ce connectivity with the next nearest neighbors is expected, compared to cases with the pyrochlore structure, as it forms a three-dimensional network of corner-sharing triangles (resembling a trillium flower, see Fig. 1) instead of corner-sharing tetrahedra. Within this peculiar structure, the six Ce nearest neighbors are at $d_{\text{Ce-Ce}} = 3.855(1) \text{ \AA}$ [8], which is close to a direct Ce-Ce contact. In any case, no effect is expected on the magnetic interactions owing to the chiral arrangement of the corner-shared triangles, because no net magnetic component arises from each triangle due to its intrinsically frustrated character and the system behaves as a chiral chain of nonmagnetic trimers.

II. EXPERIMENTAL DETAILS

A. Sample preparation and characterization

Polycrystalline samples of LaIrSi and CeIrSi were obtained by melting pure ingots of respective components weighted

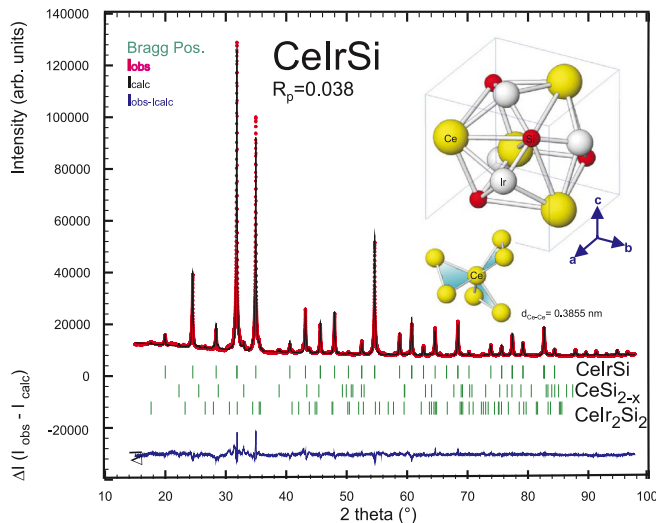


FIG. 1. Rietveld refinement of x-ray intensity data of CeIrSi. Very small amounts of CeSi_{2-x} and CeIr₂Si₂ are almost invisible (green bars below spectrum). The inset depicts the atom arrangement as well as the Ce-Ce next nearest neighbor configuration (trillium lattice).

in proper stoichiometric composition in an arc furnace with argon atmosphere, using Ti as getter material. Several remelting processes were carried out to assure sample homogeneity. Subsequently, the samples were sealed in quartz tubes and annealed for two weeks at 800 °C. X-ray powder diffraction (XRD), scanning electron microscopy (SEM), and electron probe microanalysis (EPMA) were used for the characterization of the samples.

As a derivative of the noncentrosymmetric SrSi₂-type structure [6], LaIrSi and CeIrSi compounds were found to have respective lattice parameters: $a = 6.3766(3)$ Å and $6.2951(1)$ Å. The actual relative concentration was determined by EPMA as: 33.4%, 34.7%, 31.9% for LaIrSi and 34.3%, 32.7%, 33.0% for CeIrSi. The LaIrSi sample contains small amounts (<2%) of LaIr₂Si₂ as an impurity phase [15], and CeIrSi (see the powder XRD refinement in Fig. 1) also contains about 2% of CeIr₂Si₂, CeSi_{2-x}, and small amounts of cerium oxide as impurities.

B. Magnetic, transport, and thermal measurements

The temperature dependent magnetization was measured employing a superconducting quantum interference device (SQUID) magnetometer (Cryogenic S700X) at temperatures from 0.3 to 2 K with a ³He insert and from 1.8 K to room temperature with standard ⁴He variable temperature insert and as a function of field up to 7 T.

Electrical resistivity measurements were performed employing a standard four probe configuration using an AC measurement method. Contacts were made of spot-welded gold wires with a diameter of 50 μm. Measurements were carried out down to 350 mK and magnetic fields up to 9 T.

Low temperature specific heat data were measured using two setups: (i) with a standard heat pulse technique in a semiadiabatic ³He calorimeter in the range between 0.5 and 7 K, at zero and applied magnetic field up to 4 T, and (ii) with

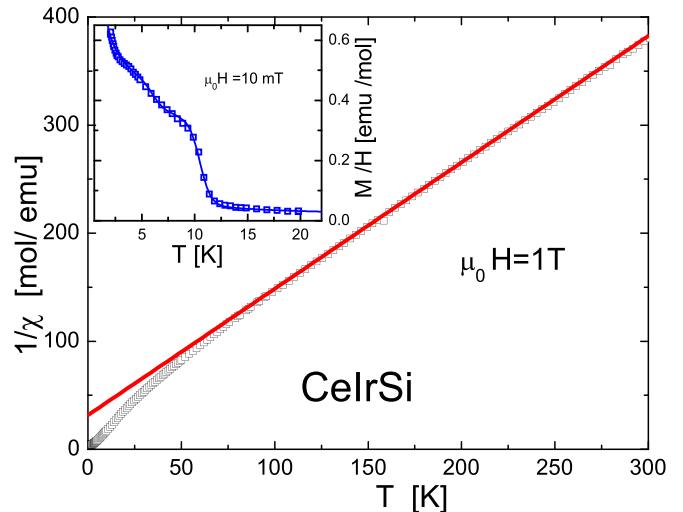


FIG. 2. Inverse susceptibility, continuous curve represents the fit according to Eq. (1). Inset: Analysis of the spurious ferromagnetic contribution below 10 K. Continuous curve shows the fit with the $M/H|_{\text{spur}}$ heuristic function described in the text.

PPMS ⁴He specific heat puck in zero field and a temperature range of 2.2 to 280 K. For this purpose, samples were prepared as a cuboid with a base of up to 2.5×2.5 mm². In general, a sample mass between 1 and 200 mg were mounted on the sample stage and attached with Apiezon-N to the platform.

III. EXPERIMENTAL RESULTS

A. Magnetic properties

1. Magnetic susceptibility

The high temperature dependent magnetic susceptibility (defined as $\chi = M/H$) in an applied field of 1 T was measured between $T = 2$ K and room temperature. The results are properly described in terms of the Curie-Weiss (CW) law, including a temperature independent contribution χ_0 :

$$\chi(T) = C/(T - \theta) + \chi_0. \quad (1)$$

Here the Curie constant $C \propto \mu_{\text{eff}}^2$; μ_{eff} is the effective magnetic moment, and θ is the paramagnetic Curie-Weiss temperature.

A least squares fit of the inverse magnetic susceptibility $1/\chi$ according to Eq. (1) above 75 K is shown as a solid curve in Fig. 2, revealing $\mu_{\text{eff}} = 2.53 \mu_B$, in accordance to the value of a free Ce³⁺ ion. The paramagnetic Curie temperature was derived as $\theta = -21$ K, suggesting antiferromagnetic (AFM) interactions among the Ce³⁺ ions, whereas the temperature independent Pauli-like contribution was found to be quite small, $\chi_0 = 1.3 \times 10^{-4}$ emu/mol. These values are in good agreement with Ref. [8] that reports a similar downwards curvature of $1/\chi$, with $\mu_{\text{eff}} = 2.56(2) \mu_B$ and $\theta = -24(1)$ K. The small difference to the present results is due to the inclusion of χ_0 in the present data evaluation, because the results from Ref. [8] are properly reproduced if the Pauli contribution is not included.

Below 60 K the inverse susceptibility significantly deviates from Curie-Weiss behavior, referring to the splitting of

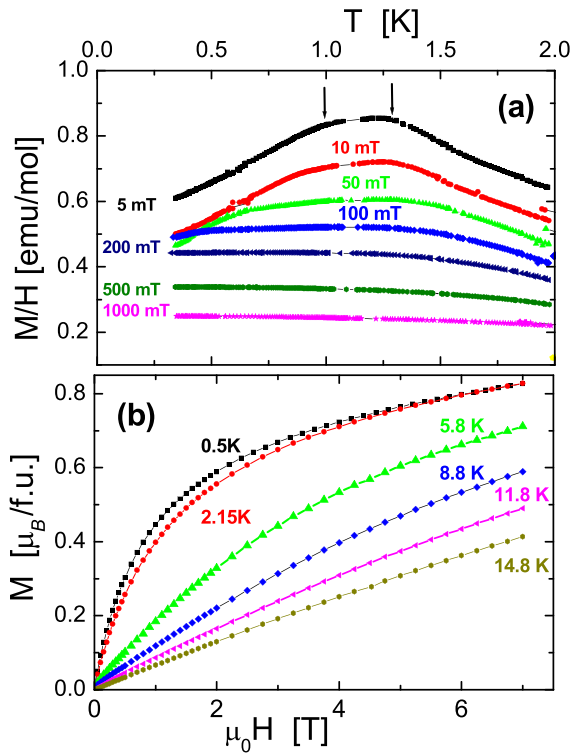


FIG. 3. (a) Low temperature magnetic susceptibility evaluated as $M/H(T)$ performed under relatively weak magnetic fields. The arrows indicate the two anomalies described in the text. The curves are shifted due to the effect of the FM contribution that arises at $T < 11$ K. (b) Low temperature magnetization measurements of CeIrSi.

the Ce^{3+} $J = 5/2$ Hund's ground state (GS) due to crystalline electric field effects. Around $T \approx 10$ K the onset of a spurious ferromagnetic (FM) signal becomes evident (see the inset in Fig. 2). Thus, the measured magnetic susceptibility below about 20 K $M/H|_{\text{meas}}$ is described using two contributions: $M/H|_{\text{meas}} = M/H|_{\text{bulk}} + M/H|_{\text{spur}}$, where $M/H|_{\text{bulk}}$ is the paramagnetic main contribution of the material: $M/H|_{\text{bulk}} = 0.33/(T - 0.3)$, and $M/H|_{\text{spur}}$ accounts for the foreign contributions. In this case, the proper fit of those contributions was obtained applying the heuristic formula $M/H|_{\text{spur}} = 0.14 \tanh(10.6 - T) + 0.045 \arctan(6 - T) + 0.23$, see the continuous curve in the inset of Fig. 2. The $M/H|_{\text{spur}}(T)$ reveals the mentioned FM contribution with $T_C = 10.6$ K attributed to the formation of a CeSi_{2-x} (with $x \approx 0.2$) solid solution [16] and a further spurious contribution centered at $T \approx 6$ K. This weak component seems to be originated by traces of Ce oxide.

Below 2 K, the low temperature magnetic susceptibility was measured in applied fields from $\mu_0 H = 5$ mT up to 1 T. In Fig. 3(a) details of the temperature dependence of $M/H(T)$ are shown around the maximum at $T \approx 1.2$ K. In this figure the curves are shifted by the effect of the FM contribution arising at $T < 11$ K, which at that low temperature can be considered practically temperature independent. A detailed analysis of the $M/H(T)$ maximum reveals a weak structure, see the two arrows in that figure. While the maximum remains nearly constant at $T \approx 1.25$ K until vanishing at

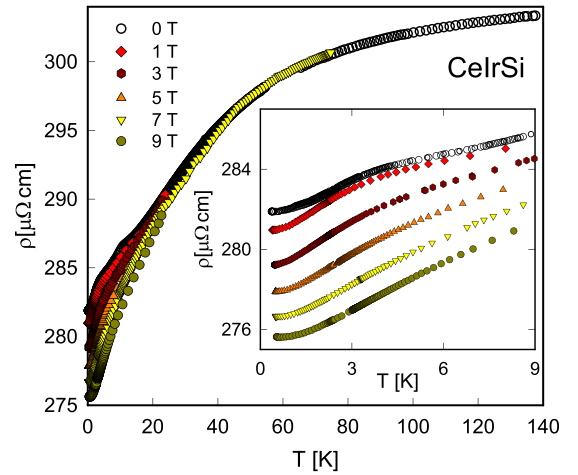


FIG. 4. Temperature and field dependent electrical resistivity measurements on CeIrSi. The inset shows the low temperature range between 0 and 12 K revealing coherent spin scattering at low temperature.

$\mu_0 H \approx 200$ mT, the kink at $T \approx 1.0$ K decreases in temperature down to $T < 0.5$ K at $\mu_0 H = 200$ mT. These features reveal a competition between two magnetic phases which are quenched at relatively low field.

2. Magnetization

The isothermal field dependence of the magnetization, measured up to $\mu_0 H = 7$ T, is included in Fig. 3(b). Only a slight variation of M vs $\mu_0 H$ is observed between 0.5 and 2.15 K, in agreement with the results presented in Fig. 3(a). The paramagnetic behavior in Fig. 3(b) can be recognized above the $T \geq 8.8$ K isotherm through the collapse of the M vs H/T curves (not shown). Strictly, isothermal curves for $T \leq 8.8$ K do not extrapolate to zero due to the spurious FM contribution, however its intensity is so low ($\approx 0.01 \mu_B/\text{f.u.}$ at 0.5 K) that it cannot be appreciated in the field scale of Fig. 3(b). According to that figure, the magnetization of CeIrSi at $T = 0.5$ K reaches $0.82 \mu_B/\text{f.u.}$ at 7 T, with a tendency of a further increase.

B. Electrical resistivity

Electrical resistivity measurements $\rho(T)$ at high temperature ($T > 140$ K) show a tendency to saturation slightly above $305 \mu\Omega \text{ cm}$ at room temperature, while from 100 to 15 K the value decreases to $288 \mu\Omega \text{ cm}$, see Fig. 4. Apart from the linear phonon contribution to $\rho(T)$, the continuous curvature can be associated with the progressive thermal population of the excited crystalline electric field levels above the ground state.

A weak kink in $\rho(T)$ around $T \approx 10.2$ K refers to the onset of long range magnetic order of ferromagnetic CeSi_{2-x} . The rather small signal change, however, indicates just a low volume fraction, which, in addition, becomes fully suppressed by rising magnetic fields (compare Fig. 4).

With decreasing temperature, the system enters into a coherent spin fluctuation regime below about 2.5 K, as evidenced by a T^2 temperature dependence of $\rho(T)$. This

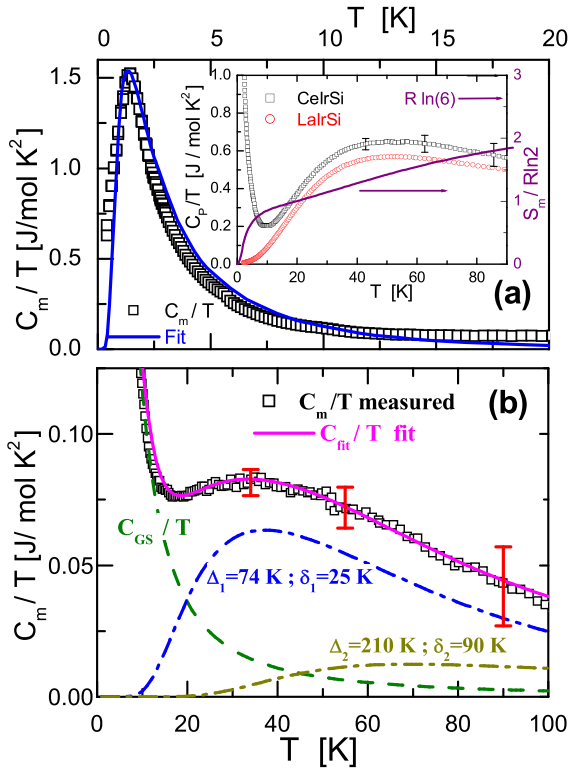


FIG. 5. (a) Low temperature magnetic contribution $C_m(T)/T$ up to 20 K and (continuous curve) comparison with theoretic prediction for a trillium-type lattice [18]. Inset: (left axis) Measured specific heat $C_p(T)/T$ of CeIrSi and LaIrSi up to 90 K and (right axis) entropy variation $S_m(T)$ normalized to a doublet GS $R \ln 2$. (b) High temperature $C_m(T)/T$ of CeIrSi showing the analysis for GS and two excited level contributions (see the text). Error bars are representative of the uncertainty of the $C_p(T)$ measurements.

regime appears to be quite robust with respect to distinct changes observed in both $C_p(T)$ and $\chi(T)$ in this temperature range.

By increasing magnetic fields the Ce spins get aligned along the external field direction and thus reduce the electrical resistivity. Notably, a negative residual magnetoresistivity $\rho_0(H)$ at $T \rightarrow 0$ shows an almost linear dependence with a small ratio $\Delta\rho_0/\Delta H \approx 0.7 \mu\Omega \text{ cm/T}$ and an expanding range of spin fluctuation type behavior. This reveals a magnetic scattering component in ρ_0 that is reduced by increasing magnetic field. On the other hand, the influence of external magnetic fields up to 9 T appears to be negligible at temperatures above 60 K.

C. Specific heat

Specific heat measurements $C_p(T)$ provide a deeper insight on the GS nature of CeIrSi. Zero field measurements, performed from 0.5 up to 90 K, are shown as C_p/T vs T in the inset of Fig. 5(a). The magnetic specific heat contribution C_m was obtained by subtracting the phonon contribution C_{ph} extracted from the isotopic compound LaIrSi [17], i.e., $C_m = C_p(\text{CeIrSi}) - C_p(\text{LaIrSi})$. At low temperature $C_p(\text{LaIrSi})$ can be described by the simple formula: $\gamma T + \beta T^3$, where $\gamma = 2.8 \text{ mJ/mol K}^2$ and $\beta = 0.672 \text{ mJ/mol K}^4$. The full range

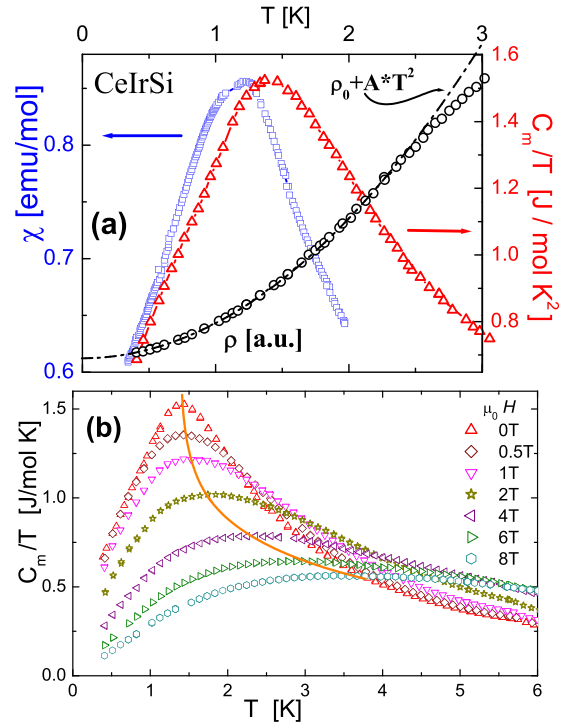


FIG. 6. (a) Comparison between $\chi(T)$, $C_m(T)/T$, and $\rho(T)$ at $T < 3$ K. (b) Specific heat dependence of CeIrSi in magnetic field up to $\mu_0 H = 8$ T. Continuous curve: Guide to the eyes tracing the $C_m(T, H)/T$ maxima.

$C_p(T)$ dependence of LaIrSi is included in the inset of Fig. 5(a).

The FM transition of CeSi_{2-x} at $T \approx 10$ K, weakly present in $\rho(T)$ measurements, is not observed in specific heat at all because of the small amount of the phase involved. The most relevant feature observed in Fig. 5(a) is the $C_m(T)/T$ maximum centered at $T^* \approx 1.5$ K that almost coincides in temperature with the maximum in the magnetic susceptibility, presented in detail in Fig. 6(a). Obviously there is no distinct specific heat jump associated to the $C_m(T)/T$ maximum: the $T > T^*$ tail shows a long monotonous decrease.

IV. DISCUSSION

A. Excited CEF levels contribution to specific heat

The analysis of the GS and the excited CEF level contributions to specific heat up to 100 K is presented in Fig. 5(b) and separated as $C_m(T)/T = C_{GS}/T + C_{CEF}/T$. Because of the C_3 (.3.) local symmetry of the $4a$ Ce sites in CeIrSi, the CEF splits the sixfold degenerate Hund's rule ground state of Ce^{3+} (total angular momentum $J = 5/2$) into three Kramer's doublets, with respective energies at Δ_1 and Δ_2 . This scenario could be described by a pair of two Schottky anomalies built up from narrow (δ -Dirac like) levels. However, due to the hybridization effects acting on CEF levels they broaden in energy and the proposed standard Schottky anomalies do not fit the $C_{CEF}(T)$ dependence properly anymore. In order to account for such a broadening, those CEF excited doublets can be approximated by two sets of levels symmetrically distributed in energy around the nominal values Δ_1 and Δ_2 .

Therefore, the general formula becomes [19]

$$C_{\text{CEF}}(T) = \sum_i \sum_j A_{i,j} \left[\left(\frac{\Delta_i \mp \delta_{i,j}}{2T} \right) / \cosh \left(\frac{\Delta_i \mp \delta_{i,j}}{2T} \right) \right]^2, \quad (2)$$

where $A_{i,j} = R \omega_i a_{i,j}$, with R being the gas constant. Coefficients ω_i indicate the degeneracy ratio between excited and ground levels: $\omega_1 = 1$ and $\omega_2 = 1/2$, respectively, whereas $a_{i,j} = 1/2$ account for the weight of each satellite level around respective Δ_i energies. In this case $|\delta_{i,1}| = |\delta_{i,2}|$ because these levels are symmetrically placed with respect to each Δ_i . Thus, according to the proposed pattern the excited CEF levels are distributed as follows: two levels at $\Delta_1 - \delta_1$ and $\Delta_1 + \delta_1$ weighted by $A_1 = 1/2R$, and two levels at $\Delta_2 - \delta_2$, and $\Delta_2 + \delta_2$ weighted by $A_2 = 1/4R$, respectively. This schematic distribution of the CEF levels mimics the broadening of each Δ_i doublet introducing a split of $\mp \delta_i$, which can be associated with the hybridization strength or Kondo temperature ($\propto T_{K_i}$) of each doublet [20].

The parameters extracted from the fit to experimental data are $\Delta_1 = 74$ K with an associated $\delta_1 = 25$ K, and $\Delta_2 = 210$ K with $\delta_2 = 90$ K. Respective contributions to specific heat are depicted in Fig. 5(b) together with the GS contribution that allows us to describe the total magnetic contribution as $C_{\text{fit}}(T)/T$. The main consequence of this analysis is to confirm that the doublet GS is energetically well separated from the first excited CEF doublet, and that both excited levels exhibit moderate hybridization effects. In order to check the validity of Eq. (2) and the proposed coefficients, we have extrapolated the fitting curve to high temperature and computed the corresponding entropy variation $S_{\text{fit}}(T)$. The expected saturation value $S_{\text{fit}} = R \ln 6$ is asymptotically reached around 500 K once all CEF levels become equally populated.

B. Low temperature properties

A theoretical prediction for a trillium-lattice system of spin-ice type behavior, studied using Monte Carlo calculations [18], is included as a solid curve in Fig. 5(a) after scaling respective C_m/T maxima. Deviations from the measured thermal dependence can be due to the finite number (six) unit cells that does not reproduce the continuous spectrum of excitations observed in the real system. In fact, measured $C_m(T)/T$ shows a nearly linear dependence with a $C_m/T|_{T \rightarrow 0} \approx 0.35$ J/mol K², whereas model calculations suggest the presence of an energy gap approaching $T = 0$. This different way to approach zero T explains why the expected $S_m = R \ln 2$ value is practically reached in the studied compound and not by the model. At high temperature ($T \geq 10$ K) there is an incipient contribution of the excited CEF levels, neither included into the model. Thus, $C_m/T(T \geq 10$ K) exceeds the Monte Carlo simulation data. In Ref. [15] specific heat is presented as a function of the coupling constant J intensity: Temperature (units of J), with the maximum value at $J/2$. Therefore the observed maximum at 1.4 K in measured $C_m(T)$ corresponds to a $J \approx 3$ K value.

A comparison between $\chi(T)$, $C_m(T)/T$, and $\rho(T)$ is presented in Fig. 6(a). Notably both $\chi(T)$ and $C_m(T)/T$ maxima, centered between $T_{\text{max}} = 1.3$ and 1.5 K, respectively,

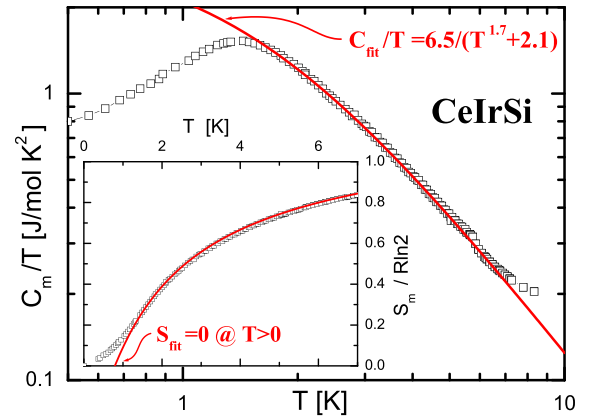


FIG. 7. Double logarithmic representation showing the thermal dependence of $C_m(T)/T$ above the maximum and the corresponding power-law fit (solid curve). Inset: Thermal dependence of the entropy compared with the extrapolation of $S_{\text{fit}}(T)$ to zero (solid line) at finite temperature.

occur within the range at which $\rho(T) \propto T^2$, below $T_{\text{coh}} \approx 2.5$ K. The robustness of the magnetic moments indicates that screening due to the Kondo effect is quite low in this compound. Coincidentally, the ground state CW temperature (θ_{GS}) extrapolated from the $20 > T > 10$ K range is $\theta_{\text{GS}} \approx 1$ K. There is however a coherent range of the electrical resistivity (i.e., AT^2) at $T < T_{\text{coh}} \approx 2.5$ K that may indicate the onset of spin fluctuations like in UPt₃ [21].

Together with the lack of a $C_m(T)/T$ jump, this behavior excludes $\chi(T)$ and $C_m(T)/T$ maxima as due to a standard phase transition. To gain insight into the magnetic character of the GS, we have performed specific heat measurements under magnetic fields up to $\mu_0 H = 8$ T, see Fig. 6(b). The maximum of $C_m(T, H)/T$ decreases and slightly shifts to higher temperature up to $\mu_0 H \approx 2$ T. The solid line in Fig. 6(b) describes the evolution of the maximum, which broadens once the applied field starts to polarize the GS spins above $\mu_0 H \approx 4$ T.

C. Entropy trajectory and magnetic frustration

In order to analyze the nature of the low temperature anomaly presented in Fig. 6, one may compare this behavior with similar ones observed in other intermetallics [22]. A common feature of those systems is the power-law thermal dependence of $C_m(T)/T$ above its maximum. In Fig. 7 this feature is verified in a double logarithmic representation, where the measured values are accounted for by a modified power law $C_{\text{fit}}/T = 6.5/(T^{1.7} + 2.1)$ J/mol K². Such a thermal dependence is comparable with that observed in compounds recognized as frustrated systems [22]. A physical interpretation of the parameters extracted from fitting the formula $C_{\text{fit}}/T = g/(T^q + a)$ is the following: the g/a ratio allows us to evaluate the density of states $C_m/T|_{T \rightarrow 0} = 6.5/2.1 \approx 3.2$ J/mol K² extrapolated from the paramagnetic phase at $T > T_{\text{max}}$. Moreover, the term $a = 2.1$ provides information about the scale of energy of any eventual interaction preventing the power law to diverge at $T \rightarrow 0$. Due to the $q = 1.7$ exponent, this parameter corresponds to ≈ 1.5 K, that nearly coincides with the temperature of the $C_m(T)/T$ maximum.

Differently from those recognized as spin glasses, with a $C_m(T) \propto 1/T^2$ tail at high temperature, one notices that the present fitted power-law dependence holds up very close to the maximum, with a clearly different exponent: 1.7 instead of 3 for the spin glass in a $C_m(T)/T$ representation. Furthermore, the $\rho \propto T^2$ dependence observed in this compound is not the expected for a spin glass [23].

In frustrated systems, the $C_m(T)/T$ maximum was associated with the temperature at which the thermal trajectory, represented by $C_{\text{fit}}(T > T_{\text{max}})/T$ in Fig. 7 as a solid curve, changes because of thermodynamic constraints. If $C_m(T)/T$ followed the trajectory described by $C_{\text{fit}}(T < T_{\text{max}})/T$ (solid red line in Fig. 7) it would reach unphysical values at $T \rightarrow 0$. As a consequence, the entropy evaluated as $S_{\text{fit}} = \int C_{\text{fit}}/T dT$ would exceed the available degrees of freedom ($R \ln 2$) for a doublet ground state.

An alternative description can be done analyzing the actual trajectory of the entropy shown in the inset of that figure. Here it is obvious that, if the $T > T_{\text{max}}$ values of S_{fit} are scaled with measured $S_m(T > T_{\text{max}})$, then $S_{\text{fit}} \rightarrow 0$ at $T > 0$ which is not allowed by thermodynamics. Note that in the inset of Fig. 7, the high temperature value of S_{fit} refers to $R \ln 2$ because of the scaling procedure. In such a scenario, the Nernst postulate imposes $S_m(T) \rightarrow 0$ at $T = 0$, undergoing an inflection point, where this sort of “entropy bottleneck” occurs [22]. This fact indicates that the $C_m(T)/T$ maximum is driven by a thermodynamic constraint instead of classical magnetic interactions effect.

Divergent power laws of the $C_m(T)/T$ dependence are a characteristic of frustrated systems, because low energy magnetic excitations strongly accumulate at $T \rightarrow 0$. This is due to the fact that no order parameter, able to reduce the GS degeneracy, can develop. Since entropy accumulation cannot exceed the available degrees of freedom provided by the doublet GS, the system is forced into an alternative minimum of the free energy [24]. Since this transition occurs in a continuous way, no discontinuity (or jump) is observed in $C_m(T)/T$, while such a discontinuity is observed in $\partial C_m/\partial T$, i.e., the third

derivative of the free energy. Even the faint structure observed in the magnetic susceptibility between 1 and 1.2 K may reveal a competition between two broad minima in the free energy which are blurred out by moderate magnetic fields. The origin of such an entropy bottleneck can be understood in the context of magnetic frustration of magnetic interactions due to the peculiar geometrical arrangements in the crystalline unit cell, like the 3D network of corner-sharing triangles presented in Fig. 1.

V. CONCLUSIONS

The peculiar trillium type crystalline structure of CeIrSi provides the possibility to study the effects of magnetic frustration in a 3D Ce lattice. The entropy driven character of the anomaly, observed around 1.3 K, is deduced from the divergent power-law dependence of $C_m(T)/T$. At that temperature, the entropy is constrained to change the trajectory in order to not overcome the $S_m = R \ln 2$ limit imposed by the Nernst postulate. Notably, there is a number of compounds showing similar $C_m(T)/T$ anomalies, followed by very similar power-law dependencies at higher temperature [22], all of them are related to underlying frustration features. The present compound, with a trillium type structure, exhibits the same spin-ice character than pyrochlore structured ones, cf. $\text{Dy}_2\text{Ti}_2\text{O}_7$, suggesting that magnetically frustrated paramagnets slide into an alternative free energy minimum driven by entropy constraints.

The $\rho \propto T^2$ dependence along the range where $\chi(T)$ and $C_m(T)/T$ maxima show up, reveals that the nature of random interactions occurring in a magnetically frustrated configuration clearly differs from a spin glass scenario. Despite some common features related to disordered interactions, like the effect of magnetic field observed in the $M(T)/H$ and $C_m(T)/T$ dependence around respective maxima may arise, the electron-spin scattering coherence of frustrated systems reveals distinct differences between dynamic and frozen landscapes.

-
- [1] D. Schiferl, *J. Chem. Phys.* **52**, 3234 (1970).
 [2] R. Moessner and J. T. Chalker, *Phys. Rev. B* **58**, 12049 (1998).
 [3] Z. Hiroi, K. Matsuhira, and M. Ogata, *J. Phys. Soc. Jpn.* **72**, 3045 (2003).
 [4] J. G. Sereni, M. Giovannini, M. Gómez Berisso, and F. Gastaldo, *J. Phys.: Condens. Matter* **28**, 475601 (2016).
 [5] S. M. Disseler, J. N. Svensson, S. C. Peter, C. P. Byers, C. Baines, A. Amato, S. R. Giblin, P. Carretta, and M. J. Graf, *Phys. Rev. B* **84**, 174429 (2011).
 [6] K. Klepp and E. Parthé, *Acta Crystallogr. Sect. B* **38**, 1541 (1982).
 [7] B. Chevalier, P. Lejay, A. Cole, M. Vlasse, and J. Etourneau, *Solid State Commun.* **41**, 801 (1982).
 [8] B. Heying, R. Pöttgen, M. Valldor, U. C. Rodewald, R. Mishra, and R.-D. Hoffmann, *Monatsh. Chem.* **135**, 1335 (2004).
 [9] D. Adroja, B. Padalia, S. Malik, R. Nagarajan, and R. Vijayaraghavan, *J. Magn. Magn. Mater.* **89**, 375 (1990).
 [10] D. G. Franco, Y. Prots, C. Geibel, and S. Seiro, *Phys. Rev. B* **96**, 014401 (2017).
 [11] T. Sakakibara, S. Nakamura, S. Kittaka, M. Kakihana, M. Hedo, T. Nakama, and Y. Onuki, *J. Phys. Soc. Jpn.* **88**, 093701 (2019).
 [12] Y. Homma, M. Kakihana, Y. Tokunaga, M. Yogi, M. Nakashima, A. Nakamura, Y. Shimizu, D. Li, A. Maurya, Y. J. Sato, F. Honda, D. Aoki, Y. Amako, M. Hedo, T. Nakama, and Y. Onuki, *J. Phys. Soc. Jpn.* **88**, 094702 (2019).
 [13] M. Kakihana, D. Aoki, A. Nakamura, F. Honda, M. Nakashima, Y. Amako, T. Takeuchi, H. Harima, M. Hedo, T. Nakama, and Y. Onuki, *J. Phys. Soc. Jpn.* **88**, 094705 (2019).
 [14] C. B. Shoemaker and D. P. Shoemaker, *Acta Crystallogr.* **18**, 900 (1965).
 [15] I. Zeiringer, Ph.D. thesis, University of Vienna, 2015, <https://othes.univie.ac.at/36084>.

- [16] H. Yashima, C. Feng lin, T. Satoh, H. Hiroyoshi, and K. Kohn, *Solid State Commun.* **57**, 793 (1986).
- [17] F. Kneidinger, Ph.D. thesis, TU Wien, 2014, <http://katalog.ub.tuwien.ac.at/AC11566341>.
- [18] T. E. Redpath and J. M. Hopkinson, *Phys. Rev. B* **82**, 014410 (2010).
- [19] J. G. Sereni, P. Pedrazzini, M. Gómez Berisso, A. Chacoma, S. Encina, T. Gruner, N. Caroca-Canales, and C. Geibel, *Phys. Rev. B* **91**, 174408 (2015).
- [20] H. Michor, J. G. Sereni, M. Giovannini, E. Kampert, L. Salamakha, G. Hilscher, and E. Bauer, *Phys. Rev. B* **95**, 115146 (2017).
- [21] M. S. Wire, J. D. Thompson, and Z. Fisk, *Phys. Rev. B* **30**, 5591 (1984).
- [22] J. G. Sereni, *J. Low Temp. Phys.* **179**, 126 (2015).
- [23] J. A. Mydosh, *Spin Glasses: An Experimental Introduction* (CRC, London, 1993).
- [24] J. G. Sereni, *J. Low Temp. Phys.* **190**, 1 (2018).